Imaging the colliding Indian and Asian lithospheric plates beneath Tibet

Prakash Kumar,[1,2] Xiaohui Yuan,[1] Rainer Kind,[1,3] and James Ni[4]

Received 6 July 2005; revised 21 January 2006; accepted 2 March 2006; published 16 June 2006.

[1] A high-resolution image of the base of the lithosphere from *S*-to-*P* converted seismic waves revealed the collision architecture of the Indian and Asian continental plates beneath the Tibetan Plateau. The base of the Indian lithosphere dips northward from a depth of 160 km beneath the Himalayas to a depth of 220 km just south of the Bangong suture. The base of the Asian lithosphere is nearly horizontal at the depth of 160–180 km from central to northern Tibet. There is a vertical gap of about 50 km between Indian and Asian lithospheres. Our observation of a well-defined, thick lithosphere throughout the entire plateau is not consistent with models of wholesale convective instability of a thickened mantle lithosphere, which would predict a very thin Asian lithosphere. The hypothesized sequential southward subduction of Tibetan and Asian continental lithospheres leading to the growth of the Tibetan Plateau, if correct, cannot be occurring below ~180 km depth. Our results, along with available geological and geophysical data, strongly support that the plateau is predominantly formed by a relatively coherent north dipping subducted Indian continental lithosphere in the south, which presently can be traced to the middle of the plateau, and a south dipping subducted Asian lithosphere in the north at a shallower depth.

Citation: Kumar, P., X. Yuan, R. Kind, and J. Ni (2006), Imaging the colliding Indian and Asian lithospheric plates beneath Tibet, *J. Geophys. Res.*, *111*, B06308, doi:10.1029/2005JB003930.

1. Introduction

[2] The Himalayan-Tibetan orogen is a result of the collision and subsequent penetration of the Indian lithosphere into the Asian lithosphere starting around 55 Ma ago [*Patriat and Achache*, 1984; *Besse et al.*, 1984]. Numerous models have been proposed to explain the formation of Tibetan Plateau. The structure of the lithosphere, especially its mantle part, is still debated. The most fundamental question concerning the deformation of this orogen is whether convergence between India and Asia was accommodated in the continental mantle lithosphere by homogeneous thickening or subduction. Mapping of the lithosphere-asthenosphere boundary (LAB), the base of the lithosphere, beneath the Tibetan Plateau has the potential to address this question. This boundary is significant in calculation of mantle dynamics [*Jordan*, 1981]. The terms lithosphere and asthenosphere were originally defined with regards to rheology, with the lithosphere behaving essentially as elastic solid, and the asthenosphere deforming as a viscous fluid [*Barrell*, 1914]. Since then additional usages of the term lithosphere have been introduced such as thermal, seismic or chemical lithosphere [*Anderson*, 1995]. Observations of low seismic velocities in the upper mantle are interpreted as being indicative of the asthenosphere. The boundary between the lithosphere and the asthenosphere might be controlled by temperature and composition. So far most information about the thickness of the lithosphere comes from surface wave observations.

[3] The mode of convergence between India and Asia has been attributed to (1) subducting of the Indian continental lithosphere horizontally beneath the plateau [*Argand*, 1924; *Powell and Conaghan*, 1975; *Ni and Barazangi*, 1984], (2) homogeneous thickening of a hot and weak Tibetan crust and mantle lithosphere; [*Dewey and Burke*, 1973; *Toksoz and Bird*, 1977], (3) escape tectonics, the lateral extrusion of thickened blocks along major strike-slip faults [*Molnar and Tapponnier*, 1975; *Tapponnier and Molnar*, 1977] and (4) injection of the Indian crust into the Tibetan crust with delamination of the Indian mantle lithosphere [*Zhao and Morgan*, 1987]. The last episode of uplift since late Miocene appears to be related to the initiation of the Indian monsoon [*Molnar et al.*, 1993]. The convective instability of a thickened Asian mantle lithosphere model [*Houseman et al.*, 1981] would conveniently explain such a broad and uniform uplift. If such a regional convective downwelling did occur in the geological past along with significant thinned continental lithosphere beneath the plateau, then this process would predict a shallow LAB (thin lithosphere) in parts of Tibet. In contrast, homogeneous thickening of the Asian lithosphere would result in a thick lithosphere there, while subduction of the Indian or/and Asian

[1] GeoForschungsZentrum Potsdam, Potsdam, Germany.
[2] Now at National Geophysical Research Institute, Hyderabad, India.
[3] Also at Fachbereich der Geowissenschaften, Freie Universität Berlin, Berlin, Germany.
[4] Department of Physics, New Mexico State University, Las Cruces, New Mexico, USA.

0148-0227/06/2005JB003930$09.00

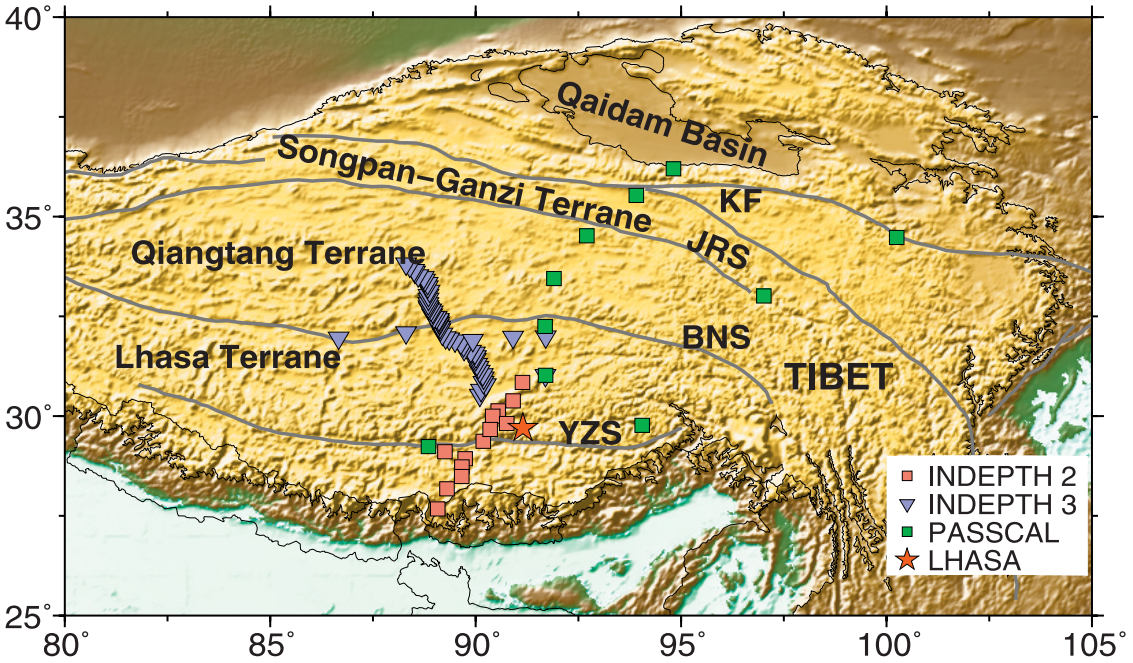

Figure 1. Topographic map of Tibet with locations of seismic stations. Seismic stations of different experiments are marked by different symbols. The main tectonic boundaries dividing Tibet into different terranes are marked: YZS, Yarlung-Zangbo suture; BNS, Bangong-Nujiang suture; JRS, Jinsha River suture; and KF, Kunlun fault.

continental lithosphere would predict an uneven LAB and an offset in the LAB between Indian and Asian lithospheres.

[4] The Tibetan crust is generally well imaged and it is widely accepted that the crustal thickness is about double that of the normal crust [e.g., *Kind et al.*, 2002]. In contrast, the thickness of the lithosphere is only known with low resolution from surface wave dispersion studies [e.g., *Romanowicz*, 1982; *Rapine et al.*, 2003; *Zhu et al.*, 2002; *Friederich*, 2003; *Huang et al.*, 2003]. The detection of LAB with higher-resolution seismic body waves (*P* or *S* phases) is still a challenging task. Recently a technique employing *S*-to-*P* converted body waves (the *S* receiver function technique) has been developed that can be used to identify the LAB with a higher resolution. This technique is a modernized version of an old technique that uses teleseismic *S*-to-*P* converted waves to detect seismic discontinuities beneath a seismic station. The main difference to the old technique is that significantly large amount of digital data are available now, permitting more sophisticated processing techniques. The *S* receiver function technique is developed from the *P* receiver function method dealing with *P*-to-*S* conversions. *P*-to-*S* conversions of the lithosphere-asthenosphere boundary are often obscured by crustal multiples, which are, however, separated from the primary conversions in the *S* receiver functions. The *S* receiver function technique is now being used more frequently to study upper mantle discontinuities [*Farra and Vinnik*, 2000; *Li et al.*, 2004; *Vinnik et al.*, 2004; *Kumar et al.*, 2005a, 2005b]. *S*-to-*P* converted phases of the Moho and the LAB are observed beneath oceans in the vicinity of Hawaii [*Li et al.*, 2004], Iceland and the northwest Atlantic [*Vinnik et al.*, 2005; *Kumar et al.*, 2005a] and beneath continents in Tien Shan and Karakoram [*Oreshin et al.*, 2002; *Kumar et al.*, 2005b]. In this study we observed two prominent discontinuities in *S* receiver functions: the crust-mantle boundary (Moho) and a second deeper discontinuity with reversed polarity. We have interpreted the latter discontinuity as LAB, although it is not trivial to identify a seismic discontinuity with a mechanical or thermal boundary.

2. Data Analysis and Methodology

[5] We examined *S*-to-*P* conversions of teleseismic broadband data sets of the 1991–1992 Tibet experiment

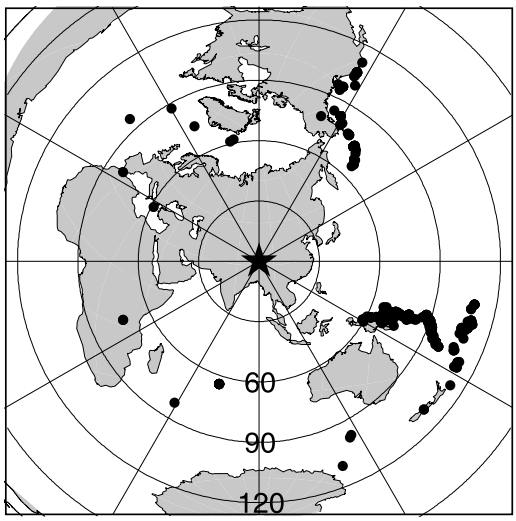

Figure 2. Location of the events used in the present study. The *S* receiver functions have been computed for the epicentral distance range of 60–85, and for *SKS* receiver functions the events from 85 to 120 have been used.

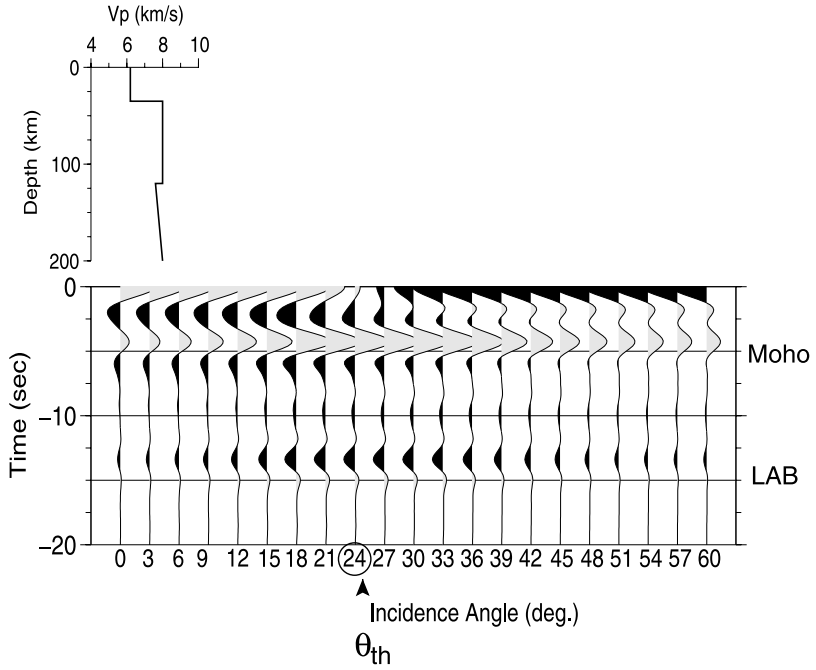

Figure 3. Determination of the angle of incidence for theoretical seismograms for a one-dimensional model (*P* component) by rotation of vertical and radial components for various incidence angles. The full wave synthetic seismograms have been generated using the version of the reflectivity method by *Wang* [1999] at an epicentral distance of 63 for a simple model shown at the top with a small velocity contrast at a negative boundary below the Moho. The receiver functions have been computed using different angles of incidence. The amplitude at the *S* arrival time (zero time) changes sign and is minimized at the correct angle of incidence (Q_{th}).

[*Owens et al.*, 1993], the international 1994 and 1998–1999 INDEPTH II and III experiments [*Nelson et al.*, 1996; *Kind et al.*, 2002] and the permanent Chinese Digital Seismic Network station LSA, located at Lhasa [*Butler et al.*, 2004]. The station locations are shown in Figure 1. We computed *S* receiver functions for all high-quality data from earthquakes within the epicentral distance range of 60–85 for *S* phases and 85–120 for *SKS* phases (see Figure 2). The processing techniques for *S* and *SKS* receiver functions are very similar to conventional *P* receiver function processing. The technique of *S* receiver functions is described by *Farra and Vinnik* [2000] and *Yuan et al.* [2006].

[6] An important step in receiver function processing is the rotation of the recorded *Z*, *N* and *E* components into a coordinate system, which enhances the converted phases. In *P* receiver functions, sometimes just the *N* and *E* components are rotated into the radial and transverse (*R* and *T*) components. A better method especially for small delay times in the *P* coda is the rotation into the local ray coordinate system *P*, *SV* and *SH*, which adds a second rotation around the angle of incidence. In *S* receiver functions the *S*-to-*P* conversions are sometimes sought on the vertical component [e.g., *Wittlinger et al.*, 2004]. For *S* receiver functions we also prefer a second rotation around the angle of incidence. The advantage of this rotation is demonstrated in Figures 3 and 4. Figure 3 shows theoretical *P* components for different rotation angles of a simple model with Moho and LAB. At the theoretical angle of incidence Q_{th} the *S* energy (at zero time) is zero. The *S* phase changes sign as a function of the angle of incidence. The Moho and LAB have their maximum (or minimum) at the theoretical angle of incidence. Moho and LAB are clearly weaker at zero angle of incidence (vertical component). This can even be seen more clearly in Figure 4 for observed data. The theoretical angle of incidence (arrow) is not always very close to the angle of incidence where *S* is changing its sign (or has a minimum). Therefore we prefer as rotation angle for which the *S* wave changes its sign (or shows a minimum). Sometimes, in unclear cases we also look for a maximum of the Moho signal, because the angle of incidence for the Moho conversion is not very much different to that for the LAB conversion. Earlier, this methodology has been used by *Kumar et al.* [2005a, 2005b] in northwest Atlantic and as well as in Tien Shan and Karakoram regions to map the LAB unprecedented details. Circles in Figure 4 mark the angles selected for rotation for that particular event. In none of the cases shown in Figure 4 is the vertical component (zero angle of

Figure 4. Determination of optimal incidence angle for *Sp* signals by rotation of the *R* and *Z* components into the *P* and *SV* components: (a–k) (top plots) earthquake records and (a–k) (bottom plots) *P* component receiver functions for different angles of incidence. The arrow indicates the theoretical angle of incidence, and the circle marks the optimum angle of incidence according to our definition. (l) Map showing the location of stations used in Figures 4a–4k.

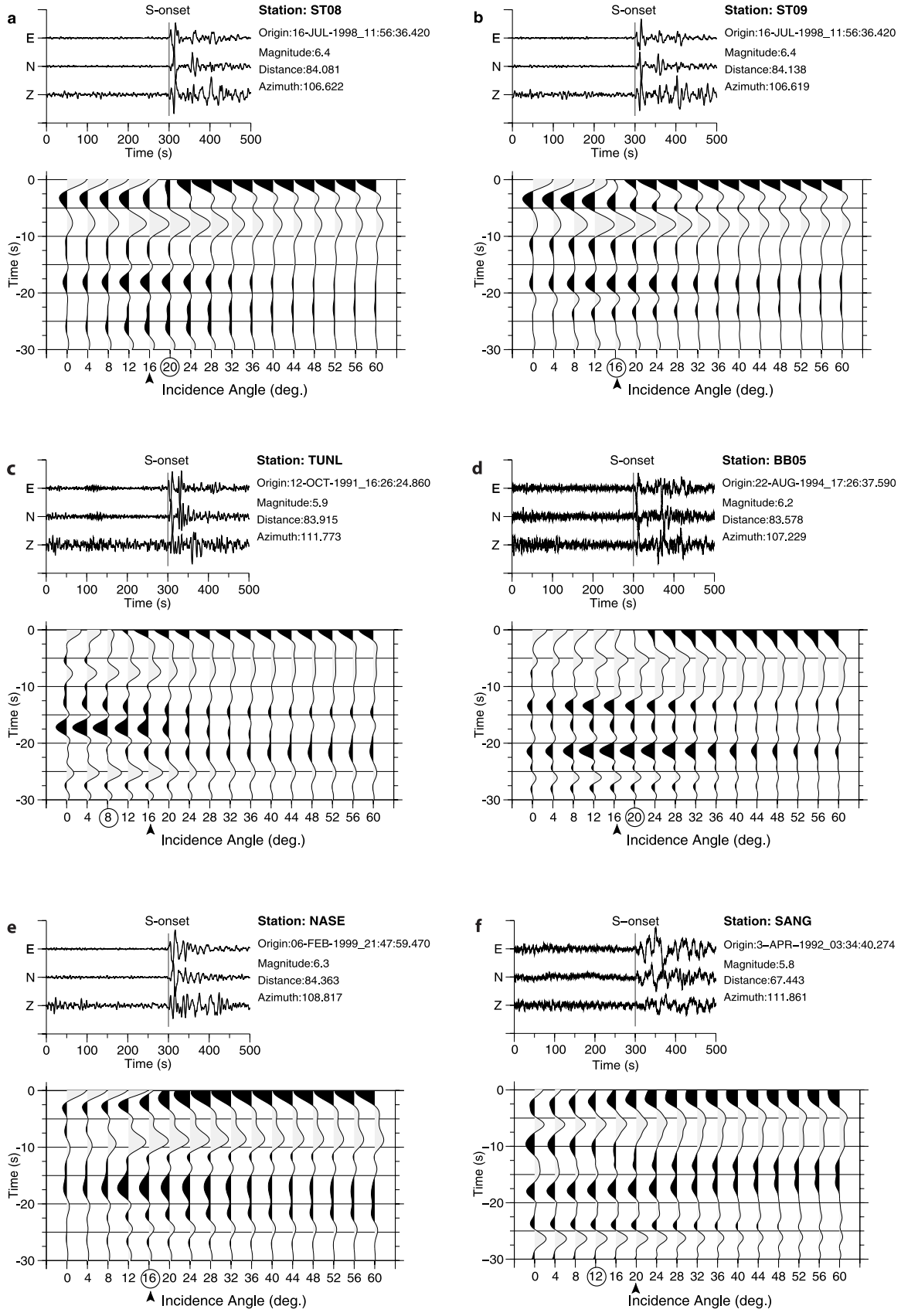
a
S-onset
Station: ST08
Origin:16-JUL-1998_11:56:36.420
Magnitude:6.4
Distance:84.081
Azimuth:106.622
E
N
Z
Time (s)
Time (s)
Incidence Angle (deg.)
b
S-onset
Station: ST09
Origin:16-JUL-1998_11:56:36.420
Magnitude:6.4
Distance:84.138
Azimuth:106.619
Time (s)
Incidence Angle (deg.)
c
S-onset
Station: TUNL
Origin:12-OCT-1991_16:26:24.860
Magnitude:5.9
Distance:83.915
Azimuth:111.773
Time (s)
Incidence Angle (deg.)
d
S-onset
Station: BB05
Origin:22-AUG-1994_17:26:37.590
Magnitude:6.2
Distance:83.578
Azimuth:107.229
Time (s)
Incidence Angle (deg.)
e
S-onset
Station: NASE
Origin:06-FEB-1999_21:47:59.470
Magnitude:6.3
Distance:84.363
Azimuth:108.817
Time (s)
Incidence Angle (deg.)
f
S-onset
Station: SANG
Origin:3-APR-1992_03:34:40.274
Magnitude:5.8
Distance:67.443
Azimuth:111.861
Time (s)
Incidence Angle (deg.)

Figure 4

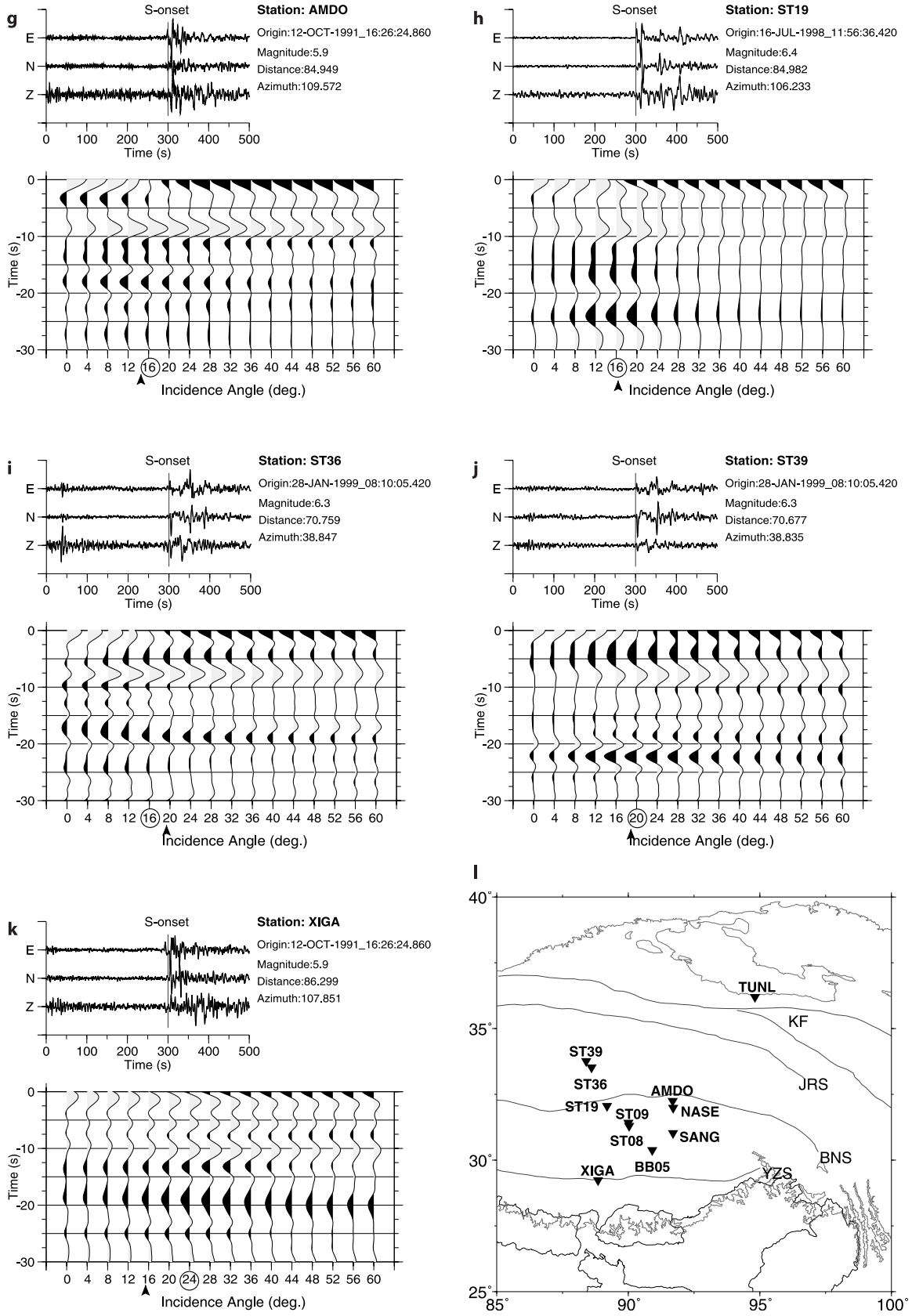

Figure 4. (continued)

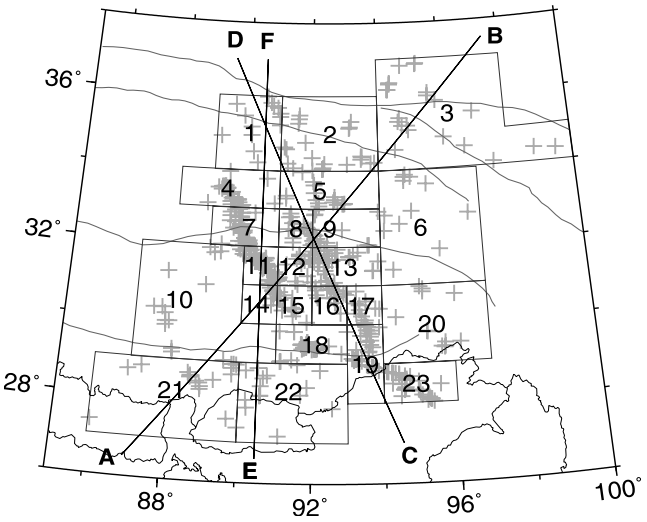

Figure 5. Crosses mark the location of piercing points of *Sp* waves at a depth of 200 km. Traces with piercing points in each of the numbered boxes have been stacked to improve the signal-to-noise ratio. Lines AB, CD, and EF are the profiles along which the boxes have been analyzed in Figures 6 and 7.

incidence) the one with strongest Moho or LAB conversions or with weakest *S* signal. Therefore we have used in all our data rotation angles determined as just described above. We experienced that using the vertical component leads to suboptimum results. We should emphasis here that in Figure 4 single event traces are shown which have rarely very good signal-to-noise ratios. That is why in receiver function technology usually summation traces are used.

[7] After rotation a deconvolution is performed in order to equalize records of different events (getting rid of different source time functions, influences of source depth and source structure and of different magnitudes and source orientations). We performed deconvolution in time domain by finding an inverse time series of the *S* phase which transforms *S* approximately into spike on the *SV* component. This inverse series is convolved with the *P* component, which results in the *S* receiver function. This step is very similar to *P* receiver function technique, except that the roles of respective components are exchanged. The remaining steps like distance moveout correction or depth migration are nearly identical to the same steps in the *P* receiver function technique. *P* and *S* receiver function techniques have profited much from techniques used in steep angle seismics.

3. Results

[8] The Sp piercing points at a depth of 200 km for all events are computed using the IASP91 model as reference [*Kennett and Engdahl*, 1991]. Figure 5 highlights the data coverage in Tibet. In order to enhance the signal-to-noise ratio the region has been divided into 23 boxes (Figure 5) and only those *S* receiver functions having piercing points within the same box are stacked. A low-pass filter with a corner frequency of 4 s before deconvolution, and a distance moveout correction were applied to the data prior to stacking. The stacked traces from each box are displayed in Figure 6. Two clear phases are visible; the Moho with positive phase (indicating velocity increase downward) and a second negative phase (indicating velocity decrease downward) labeled LAB, which we interpret as the lithosphere-asthenosphere boundary. The LAB arrives between 18 and 24 s in front of the *S* wave phase, which corresponds to a depth range between 160 and 220 km based on the IASP91 velocity model with a correction for the thick Tibetan crust. The differential times of the Moho and the LAB must be read at the maximum (or minimum) of the signal, which is due to the deconvolution. The reading error is less than 1 s, resulting in a ~10 km error in the depth determination of the LAB. The summation traces in Figure 6 are averaged over records from many distances and back azimuths within one box. The observation of well devel-

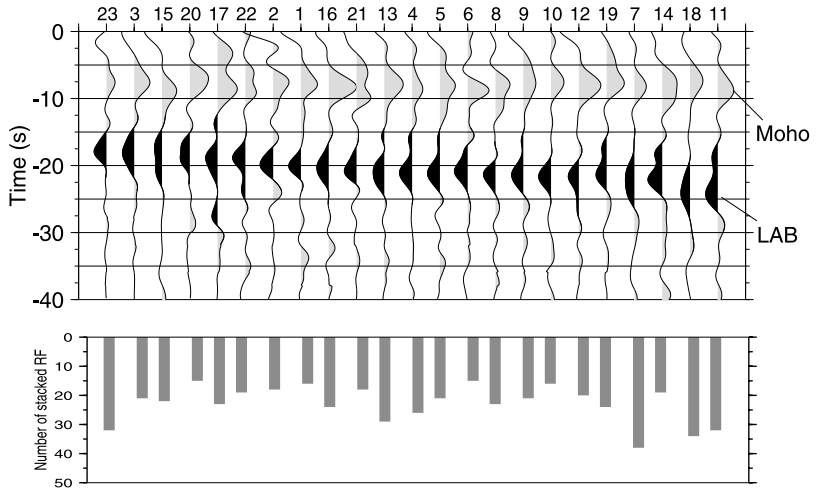

Figure 6. (top) Stacked *S* receiver functions (rotated *P* component) from each box in Figure 5. Zero time is the *S* arrival time. Timescale is reversed. Traces are sorted by increasing arrival time of the lithosphere-asthenosphere boundary (LAB) phase. Numbers on top of the traces correspond to the box numbers in Figure 5. Traces are distance moveout-corrected for a slowness of 6.4 s/degree before stacking. (bottom) Bar diagram showing number of traces summed in each box.

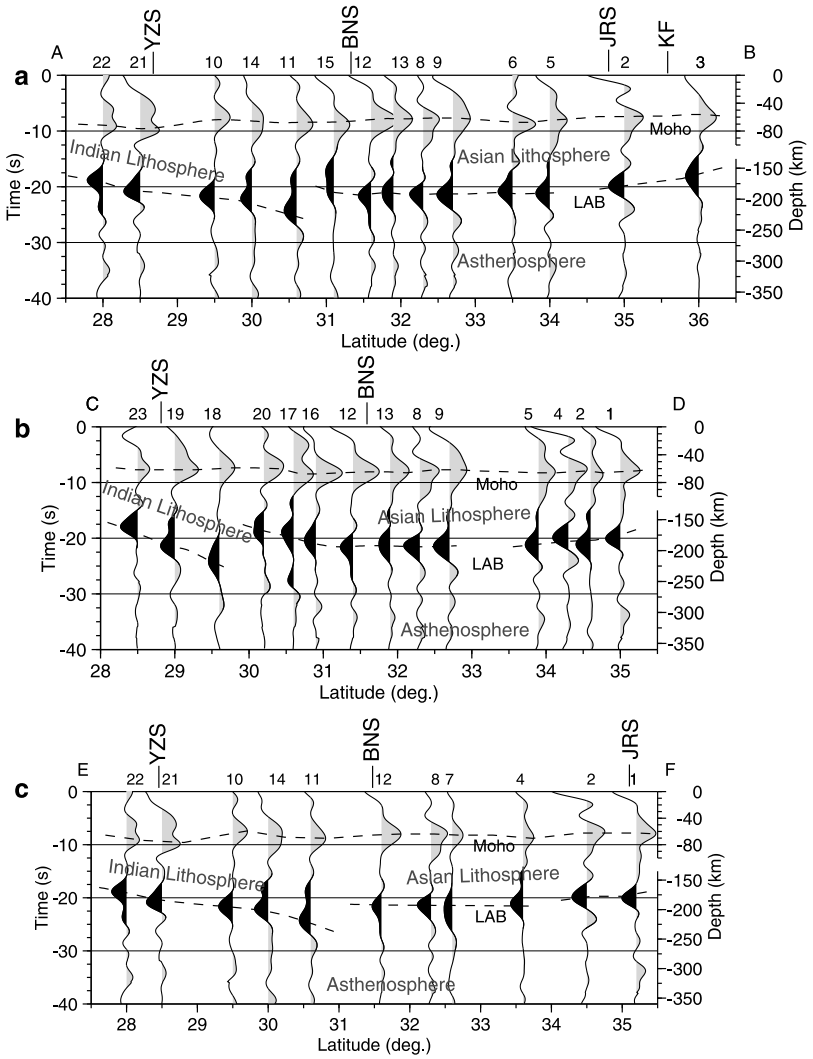

Figure 7. Stacked *S* receiver functions within the boxes in Figure 5 along the profiles (a) AB, (b) CD, and (c) EF in Figure 5. The left ordinate marks the delay time; the right ordinate is the approximate depth scale based on the standard Earth model IASP91, corrected for the Tibetan crust. The main tectonic boundaries are marked on the top of Figure 7 (see Figure 1 for full names). The Moho depth varies between 70 and 80 km across Tibet. The LAB depth varies between 160 and 220 km, with a step of about 50 km south of the BNS suture. Figures 7a–7c clearly exhibit the base of the Indian and Asian lithospheres.

oped Moho and LAB signals leads to the conclusion that topography within one box is relatively weak. How much destructive interference occurs because of discontinuity topography can only be judged by looking at individual traces. However, very good signal-to-noise ratios are required for achieving this task. The influence of anisotropy on *S* receiver functions is considerably less than on *P* receiver functions, because, we have *P* waves close to the station and not shear waves, which are influenced by possible shear wave splitting.

[9] Seismic traces have been sorted along three profiles and are shown in Figures 7 and 8. The location of these profiles is shown in Figure 5. Figure 7 displays the stacked traces within each box along the three profiles, whereas Figure 8 shows individual *S* receiver function traces adjacent to the same profiles and sorted by location of piercing points. All three profiles (Figures 7a, 7b, and 7c) show the existence of a well-imaged LAB across the entire plateau.

[10] Figure 9 shows the depth variations of the LAB in our study area. The deepest part of the LAB is found just south of the BNS and it flattens gradually toward the south and north. This deepest part is demarcating the northern (Eurasian) lithosphere from the southern (Indian) lithosphere. The crustal thickness derived from *P* receiver functions [*Kind et al.*, 2002] and from the present studies corroborates well (Figure 10). However, the timing of the LAB in *P* receiver functions (Figure 10) is heavily disturbed by the strong crustal multiples.

4. Discussion

[11] Our observed negative phase below the Moho is certainly caused by a negative discontinuity there. We have

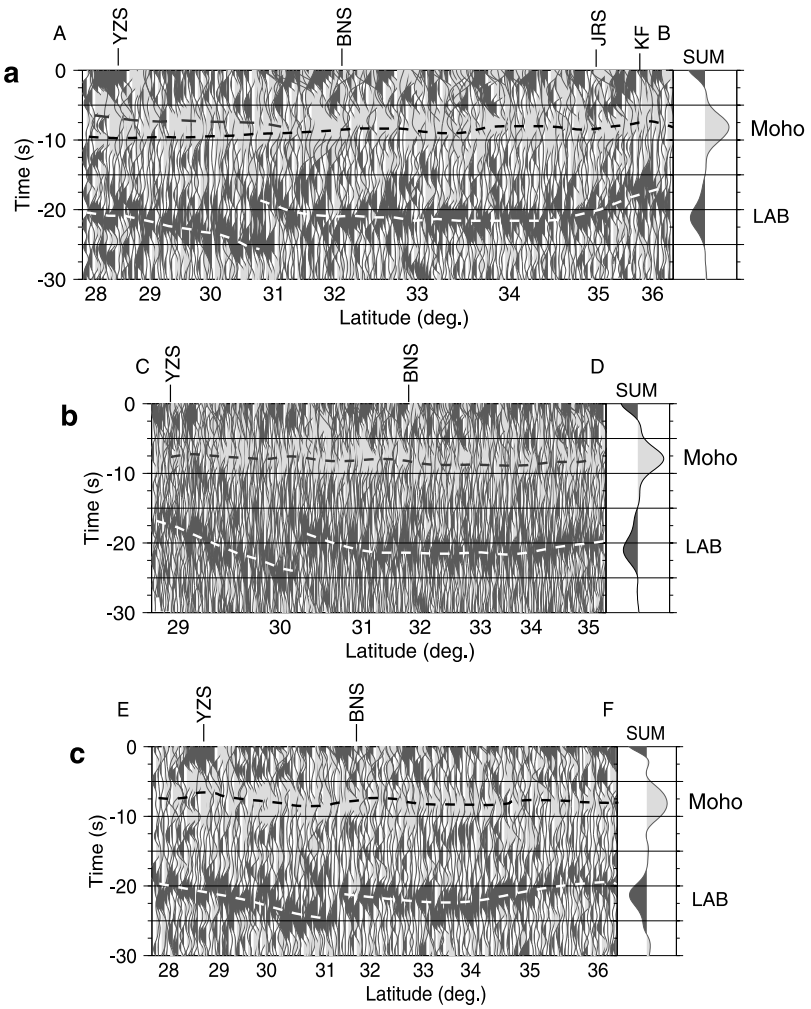

Figure 8. Individual *S* receiver function traces along the profiles (a) AB, (b) CD, and (c) EF. Stacked traces along the three profiles are shown on the right. The data have been taken along a narrow swath of about 1 half width. The individual and summed traces clearly show the two main phases: Moho (positive) and LAB (negative).

indeed observed down to nearly 300 km depth below Tibet in average only two main discontinuities, the positive Moho and the negative phase in the upper mantle (see summation traces in Figure 8). In seismology such a negative signal in the upper mantle is frequently called "Gutenberg" discontinuity [after *Gutenberg*, 1959]. The Gutenberg discontinuity is frequently identified with the LAB. The Lehmann discontinuity is thought to be deeper than the Gutenberg discontinuity. It is also considered a positive discontinuity and it is usually associated with the bottom of the asthenosphere. We have no indication for such a discontinuity in our data, down to about 300 km beneath Tibet. The low-velocity zone observed in surface waves is also frequently identified with the asthenosphere. However, we should remember that the lithosphere and asthenosphere are mechanical definitions, not seismic definitions (the Moho is in contrast a purely seismic definition). Frequently the LAB is assumed a smooth thermal transition (although chemical or petrologic changes are not excluded).

[12] The existence of a cold and strong lithosphere in southern Tibet and the Himalayas [*Ni and Barazangi*, 1983] has been established, but the nature of the lithosphere in northern Tibet is still not well known. It has been also suggested that there could be little mantle lithosphere beneath northern Tibet [*Romanowicz*, 1982]. Our observations show with good resolution the existence of a clear LAB in southern as well as in northern Tibet in the depth ranges of 160 and 220 km (Figure 11). They are separated by a step of at least 50 km between 30–31N latitude (just south of the BNS), where the Indian lithosphere is subducting below the Asian lithosphere. The nearly vertical upper mantle high-velocity body south of Bangong suture imaged by teleseismic tomography [*Tilmann et al.*, 2003] may represent the deeper part of the Indian continental lithosphere. The fast tomographic velocity at about 400 km depth could be the location of the final slab break off [*Davis and von Blanckenburg*, 1995] because of negative buoyancy resulting from increase in density by eclogitization of the subducted oceanic Indian plate. The model of convective removal of a thickened Asian lithosphere [e.g., *Houseman et al.*, 1981] could only be consistent with the upper part of the mantle lithosphere, not with the observed LAB beneath

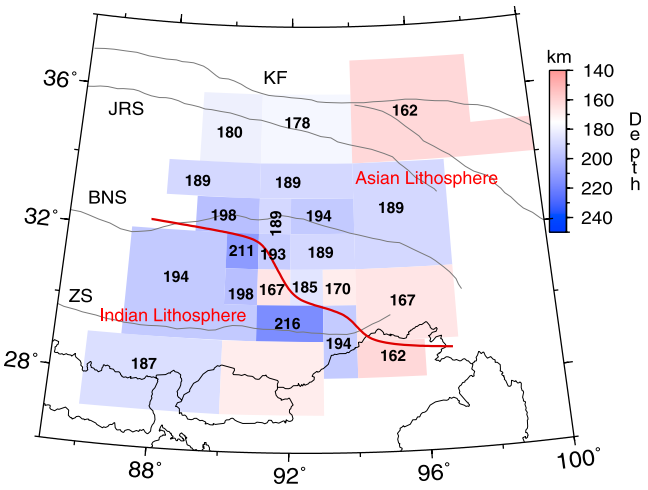

Figure 9. Depth map of the lithosphere-asthenosphere boundary in central Tibet. The lithosphere is deepest within the region bounded by the YZS and BNS. The bold red line is the boundary demarcating approximately the Indian and Asian lithospheres. The boxes correspond to the boxes shown in Figure 5. The numbers are the LAB depths in kilometers.

northern Tibet, if our interpretation is correct. The model invoking subduction of Asian lithosphere beneath northern Tibet, hypothesized by *Tapponnier et al.* [2001], cannot be extended beyond a depth of 180 km. However, there is no resolution power in our data for such a steep southward verging subduction of Asian lithosphere. A recent focal mechanism study of mantle events suggests the existence of strong lithosphere in the western Himalayan syntaxis [*Chen and Yang*, 2004] and this result is consistent with our finding of subducted Indian continental lithosphere beneath the southern Tibet and the eastern Himalayan syntaxis.

[13] Beneath northern Tibet, the base of the Asian lithosphere is subhorizontal at a depth of 160–180 km based on the modified ISAP91 model with a double crustal thickness. Although *Romanowicz* [1982] prefers the no-lid model for the northern Tibetan plateau, the pure-path Rayleigh and Love phase velocities also can be fitted by a lithospheric model with a mantle lid. A 250-km-wide low-velocity body at depths greater than 150 km has been reported by a tomographic study [*Wittlinger et al.*, 1996] south of the Kunlun range in northern Tibet. This low-velocity body has been interpreted as an upwelling mantle that is responding to the subduction of cold and dense Indian continental lithosphere [*Tilmann et al.*, 2003]. Previous *P* receiver

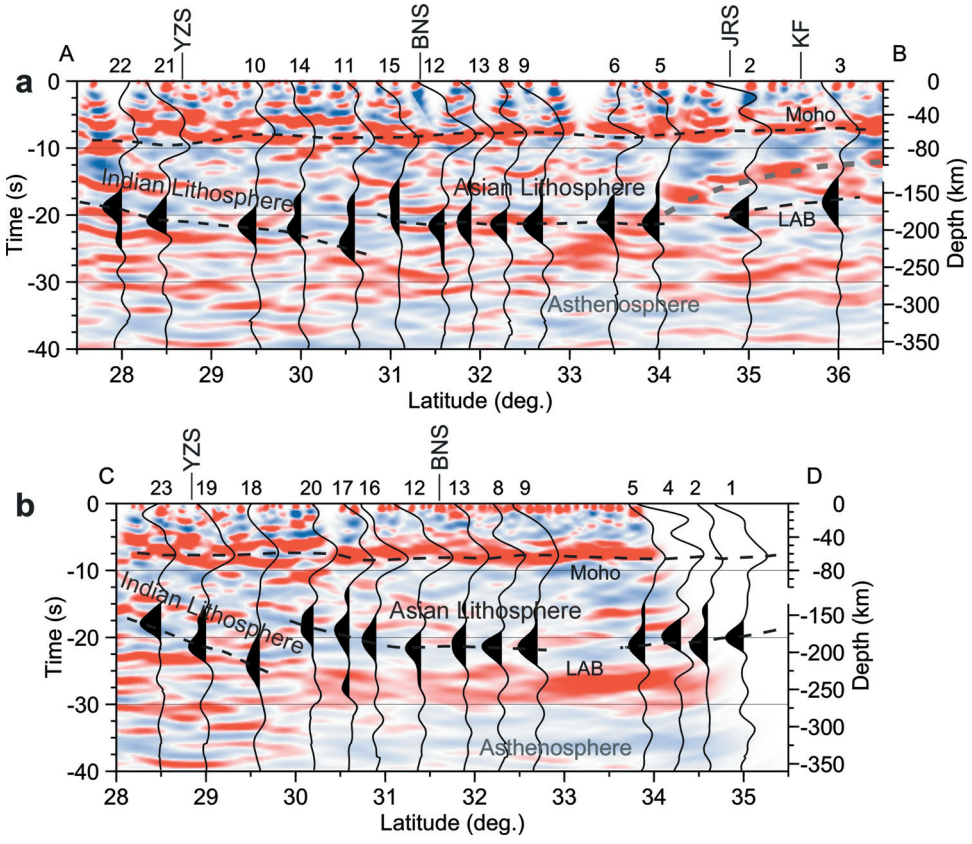

Figure 10. Superposition of *P* [*Kind et al.*, 2002] and *S* receiver functions along the two profiles (a) profile AB and (b) profile CD. *P* receiver functions are plotted in red (positive) and blue (negative). Negative amplitudes of *S* receiver functions are shaded black. The Moho boundaries of both data sets agree very well with each other. The LAB cannot be identified in the *P* receiver functions because of the ambient noise of the crustal multiples. South dipping dashed grey line in the north of Figure 10a indicates top of Asian subducting lithosphere seen in *P* receiver functions [*Kind et al.*, 2002]. This structure is not seen in *S* receiver functions probably because of sparse data in the north.

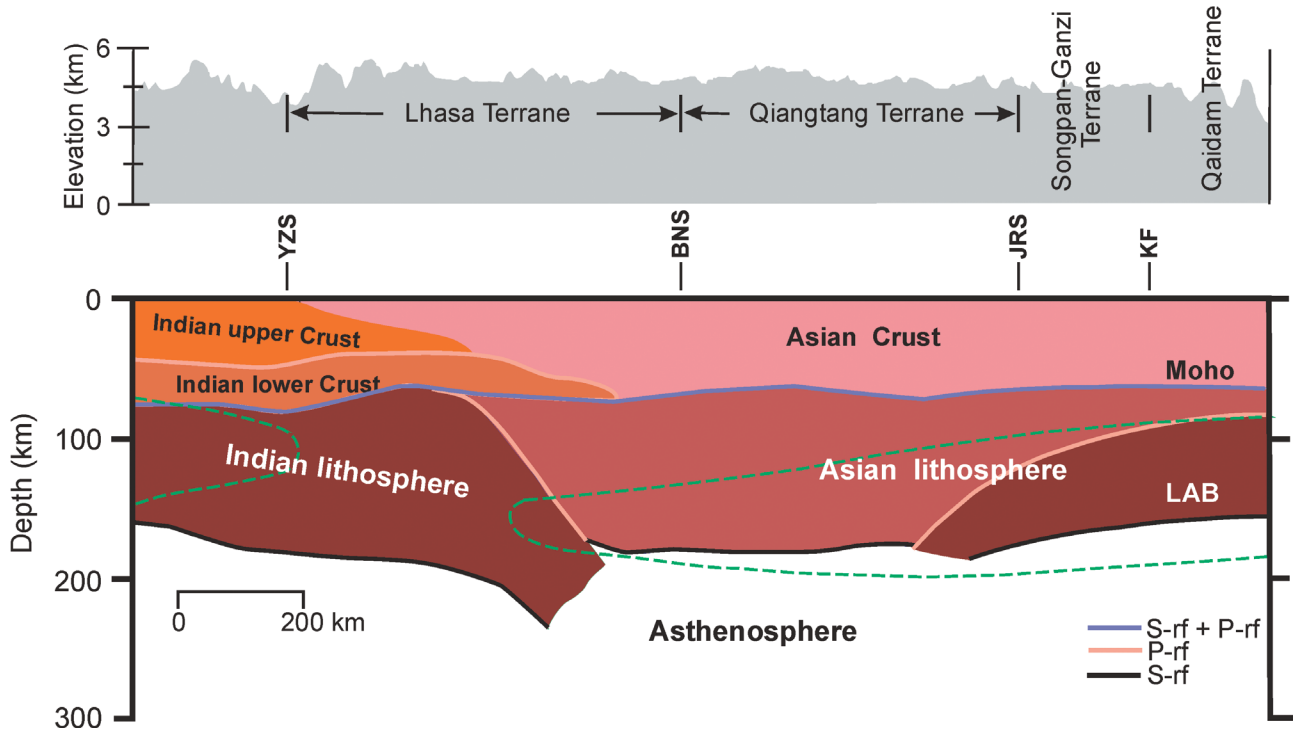

Figure 11. Sketch illustrating the collision of the Indian and Asian lithospheric plates summarizing the results of *S* receiver function (*S*-rf) analysis (this paper) and earlier *P* receiver function (*P*-rf) results. The observations suggest subduction of both the Indian and Asian lithospheres. The Indian plate is penetrating into the mantle to the south of the Bangong suture (BNS). The Asian subducting lithosphere appears also to contribute to the growth of the Tibetan plateau [*Tapponnier et al.*, 2001]. The upper boundaries of the Indian and Asian lithospheres are constrained by the *P* receiver functions [*Kosarev et al.*, 1999; *Kind et al.*, 2002], while the lower boundaries are determined by the *S* receiver functions. The Moho depth, constrained by the *P* and *S* receiver functions, varies smoothly between 80 and 60 km. *P* receiver functions indicate penetration of the Indian lower crust several hundred kilometers to the north of the Zangbo suture [*Yuan et al.*, 1997; *Kind et al.*, 2002]. Dashed lines in green indicate a zone of high shear wave velocity from the tomography study of *Griot et al.* [1998], after *Tapponnier et al.* [2001].

function observations indicate a north dipping upper boundary of the detached Indian lithosphere [*Kosarev et al.*, 1999] above the imaged subducting Indian lithosphere. A south dipping upper boundary of a detached Asian lithosphere was interpreted by *Kind et al.* [2002] north of the Bangong suture. However, both structures within the mantle lithospheres are difficult to image in our present *S* receiver function analysis. The reason could be that these features, located within the mantle lithosphere, have weaker impedance contrast than that from the Moho or LAB and are not detected by the limited data that are currently available especially in the northern Tibet.

[14] **Acknowledgments.** P.K. was supported by a stipend from the Deutsche Akademische Austauschdienst (DAAD). P.K. is also grateful to the Director, NGRI and DG, CSIR, India, for granting deputation to carry out this research work. Project INDEPTH/GEDEPTH experiments were supported by the GeoForschungsZentrum, Potsdam, the Deutsche Forschungsgemeinschaft, Continental Dynamics Program of the U.S. National Science Foundation, and the Chinese Academy of Geological Sciences. Data from the Tibet PASSCAL 1991–1992 were collected in a joint project between the University of South California (T. Owens and G. Randall), State University of New York-Binghamton (F. Wu), and the research group of R. Zeng, Institute of Geophysics, China Earthquake Administration. The data have been provided from IRIS DMS. Thanks to Doug Angus and Karen Bucher for reading the manuscript. Computations have been done in Seismic Handler (K. Stammler). We also wish to thank Geoffrey Abers, Greg Houseman, and Anne Sheehan for suggesting significant clarifications.

References

Anderson, D. L. (1995), Lithosphere, asthenosphere, and perisphere, *Rev. Geophys.*, *33*, 125–149.

Argand, E. (1924), La tectonique de l'Asie, in *Geological Congress*, *13th Proceedings*, vol. 7, pp. 71–372.

Barrell, J. (1914), The strength of the Earth's crust, *J. Geol.*, *22*, 680 ff.

Besse, J., V. Courtillot, J. P. Possi, M. Westphal, and Y. Z. Zhou (1984), Paleomagnetic estimates of crustal shortening in the Himalayan thrusts and Zangbo suture, *Nature*, *311*, 621–626.

Butler, R., et al. (2004), The Global Seismograph Network surpasses its design goal, *Eos Trans. AGU*, *85*, 23.

Chen, W.-P., and Z. Yang (2004), Earthquakes beneath the Himalayas Tibet: Evidence for strong lithospheric mantle, *Science*, *304*, 1949–1952.

Davis, J. H., and F. von Blanckenburg (1995), Slab breakoff: A model of lithosphere detachment and its test in the magmatism and deformation of collisional orogens, *Earth Planet. Sci. Lett.*, *129*, 85–102.

Dewey, J. F., and K. C. Burke (1973), Tibetan, Variscan, and Precambrian basement reactivation: Products of continental collision, *J. Geol.*, *81*, 683–692.

Farra, V., and L. Vinnik (2000), Upper mantle stratification by P and S receiver functions, *Geophys. J. Int.*, *141*, 699–712.

Friederich, W. (2003), The S-velocity structure of the east Asian mantle from inversion of shear and surface waveforms, *Geophys. J. Int.*, *153*, 88–102.

Griot, D.-A., J.-P. Montagner, and P. Tapponnier (1998), Phase velocity structure from Rayleigh and Love waves in Tibet and its neighboring region, *J. Geophys. Res.*, *103*, 21,215–21,232.

Gutenberg, B. (1959), *Physics of the Earth's Interior*, 240 pp., Elsevier, New York.

Houseman, G. A., D. P. McKenzie, and P. Molnar (1981), Convective instability of a thickened boundary layer and its relevance for thermal evolution of continental convergent belts, *J. Geophys. Res.*, *86*, 6115–6132.

Huang, Z., W. Su, Y. Peng, Y. Zheng, and H. Li (2003), Rayleigh wave tomography of China and adjacent regions, *J. Geophys. Res.*, *108*(B2), 2073, doi:10.1029/2001JB001696.

Jordan, T. H. (1981), Continents as a chemical boundary layer, *Philos. Trans. R. Soc. London, Ser. A*, *301*, 359–373.

Kennett, B. L. N., and E. R. Engdahl (1991), Traveltimes for global earthquake location and phase identification, *Geophys. J. Int.*, *105*, 429–465.

Kind, R., X. Yuan, J. Saul, D. Nelson, S. V. Sobolev, J. Mechie, W. Zhao, G. Kosarev, J. Ni, U. Achauer, and M. Jiang (2002), Seismic images of crust and upper mantle beneath Tibet: Evidence for Eurasian plate subduction, *Science*, *298*, 1219–1221.

Kosarev, G., R. Kind, S. V. Sobolev, X. Yuan, W. Hanka, and S. Oreshin (1999), Seismic evidence for a detached Indian lithospheric mantle beneath Tibet, *Science*, *283*, 1306–1309.

Kumar, P., et al. (2005a), The lithosphere-asthenosphere boundary in the north west Atlantic region, *Earth Planet. Sci. Lett.*, *236*, 249–257.

Kumar, P., X. Yuan, R. Kind, and G. Kosarev (2005b), The lithosphere-asthenosphere boundary in the Tien Shan-Karakoram region from S receiver functions: Evidence for continental subduction, *Geophys. Res. Lett.*, *32*, L07305, doi:10.1029/2004GL022291.

Li, X., R. Kind, X. Yuan, I. Wölbern, and W. Hanka (2004), Rejuvenation of the lithosphere by the Hawaiian plume, *Nature*, *427*, 827–829.

Molnar, P., and P. Tapponnier (1975), Cenozoic tectonics of Asia: Effects of a continental collision, *Science*, *189*, 419–426.

Molnar, P., P. England, and J. Martinod (1993), Mantle dynamics, uplift of the Tibetan Plateau, the Indian monsoon, *Rev. Geophys.*, *31*, 357–396.

Nelson, K. D., et al. (1996), Partially molten middle crust beneath southern Tibet: A synthesis of project INDEPTH initial results, *Science*, *274*, 1684–1688.

Ni, J., and M. Barazangi (1983), Velocities and propagation characteristics of *Pn*, *Pg*, *Sn* and *Lg* seismic waves beneath the Indian shield, Himalayan arc, Tibetan plateau, and surrounding regions: High uppermost mantle velocities and efficient Sn propagation beneath Tibet, *Geophys. J.R. Astron. Soc.*, *72*, 665–689.

Ni, J., and M. Barazangi (1984), Seismotectonics of the Himalayan collision zone: Geometry of the underthrusting Indian plate beneath the Himalaya, *J. Geophys. Res.*, *89*, 1147–1163.

Oreshin, S., L. Vinnik, D. Peregoudov, and S. Roecker (2002), Lithosphere and asthenosphere of the Tien Shan imaged by S receiver functions, *Geophys. Res. Lett.*, *29*(8), 1191, doi:10.1029/2001GL014441.

Owens, T. J., G. E. Randall, F. T. Wu, and R. Zeng (1993), PASSCAL instrument performance during the Tibetan Plateau passive seismic experiment, *Bull. Seismol. Soc. Am.*, *83*, 1959–1970.

Patriat, P., and J. Achache (1984), India-Eurasia collision chronology has implications for crustal shortening and driving mechanism of plates, *Nature*, *311*, 615–621.

Powell, C. M., and P. J. Conaghan (1975), Tectonic models for the Tibetan Plateau, *Geology*, *3*, 727–731.

Rapine, R., F. Tilmann, M. West, J. Ni, and A. Rodgers (2003), Crustal structure of northern and southern Tibet from surface wave dispersion analysis, *J. Geophys. Res.*, *108*(B2), 2120, doi:10.1029/2001JB000445.

Romanowicz, B. A. (1982), Constraints on the structure of the Tibet Plateau from pure path phase velocities of Love and Rayleigh waves, *J. Geophys. Res.*, *87*, 6865–6883.

Tapponnier, P., and P. Molnar (1977), Active faulting and tectonics in China, *J. Geophys. Res.*, *82*, 2905–2930.

Tapponnier, P., X. Zhiqin, F. Roger, B. Meyer, N. Arnau, G. Wittlinger, and Y. Jingsui (2001), Oblique stepwise rise and growth of the Tibet Plateau, *Science*, *294*, 1671–1677.

Tilmann, F., J. Ni, and INDEPTH III Seismic Team (2003), Seismic imaging of the downwelling Indian lithosphere beneath central Tibet, *Science*, *300*, 1424–1427.

Toksoz, M. N., and P. Bird (1977), Formation and evolution of marginal basins and continental plateaus, in *Island Arcs*, *Deep Sea Trenches and Back-Arc Basins*, edited by M. Talwani and W. C. Pitman III, *Maurice Ewing Ser.*, vol. 1, pp. 379–393, AGU, Washington, D. C.

Vinnik, L. P., V. Farra, and R. Kind (2004), Deep structure of the Afro-Arabian hot spot from S receiver functions, *Geophys. Res. Lett.*, *31*(11), L11608, doi:10.1029/2004GL019574.

Vinnik, L. P., G. R. Foulger, and Z. Du (2005), Seismic boundaries in the mantle beneath Iceland: A new constraint on temperature, *Geophys. J. Int.*, *160*, 533–538.

Wang, R. (1999), A simple orthonormalization method for the stable and efficient computation of Green's functions, *Bull. Seismol. Soc. Am.*, *89*, 733–741.

Wittlinger, G., et al. (1996), Seismic tomography of northern Tibet and Kunlun: Evidence for crustal blocks and mantle velocity contrasts, *Earth Planet. Sci. Lett.*, *139*, 263–279.

Wittlinger, G., V. Farra, and J. Vergne (2004), Lithospheric and upper mantle stratification beneath Tibet: New insights from Sp conversions, *Geophys. Res. Lett.*, *31*, L19615, doi:10.1029/2004GL020955.

Yuan, X., J. Ni, R. Kind, J. Mechie, and E. Sandvol (1997), Lithospheric and upper mantle structure of southern Tibet from a seismological passive source experiment, *J. Geophys. Res.*, *102*, 27,491–27,500.

Yuan, X., R. Kind, X. Li, and R. Wang (2006), The S receiver functions: Synthetics and data example, *Geophys. J. Int., Geophys. J. Int.*, *165*, 555–564.

Zhao, W.-L., and W. J. Morgan (1987), Injection of Indian crust into Tibetan lower crust: A two-dimensional finite element model study, *Tectonics*, *6*, 489–504.

Zhu, J.-S., J.-M. Cao, X.-L. Cai, Z.-Q. Yan, and X.-L. Cao (2002), High resolution surface wave tomography in east Asia and west Pacific marginal sea (in Chinese), *J. Geophys.*, *45*, 679–698.

R. Kind and X. Yuan, GeoForschungsZentrum Potsdam, Telegrafenberg, D-14473 Potsdam, Germany.

P. Kumar, National Geophysical Research Institute, Uppal Road, Hyderabad 500007, India. (prakashngri@rediffmail.com)

J. Ni, Department of Physics, New Mexico State University, Las Cruces, NM 88003, USA.